INTERNATIONAL JOURNAL FOR NUMERICAL AND ANALYTICAL METHODS IN GEOMECHANICS
Int. J. Numer. Anal. Meth. Geomech., 2002; **26**:1531–1560 (DOI: 10.1002/nag.257)

A constitutive model for granular materials with grain crushing and its application to a pyroclastic soil

Manuela Cecconi[1], Antonio DeSimone[2], Claudio Tamagnini[1] and Giulia M.B. Viggiani[3,*,†]

[1] *Università degli Studi di Perugia, via G. Duranti 93, 06125 Perugia, Italy*
[2] *Max Planck Institute for Mathematics in the Sciences, Inselstr. 22–26, 04103 Leipzig, Germany*
[3] *Università degli Studi di Roma Tor Vergata, via del Politecnico, 1, 00133 Roma, Italy*

SUMMARY

A constitutive model for granular materials is developed within the framework of strain–hardening elastoplasticity, aiming at describing some of the macroscopic effects of the degradation processes associated with grain crushing. The central assumption of the paper is that, upon loading, the frictional properties of the material are modified as a consequence of the changes in grain size distribution.

The effects of these irreversible microscopic processes are described macroscopically as accumulated plastic strain. Plastic strain drives the evolution of internal variables which model phenomenologically the changes of mechanical properties induced by grain crushing by controlling the geometry of the yield locus and the direction of plastic flow.

An application of the model to *Pozzolana Nera* is presented. The stress–dilatancy relationship observed for this material is used as a guidance for the formulation of hardening laws. One of the salient features of the proposed model is its capability of reproducing the stress–dilatancy behaviour observed in Pozzolana Nera, for which the minimum value of dilatancy always follows the maximum stress ratio experienced by the material. Copyright © 2002 John Wiley & Sons, Ltd.

KEY WORDS: pyroclastic soils; soft rocks; fabric/structure of soils; grain crushing; plasticity

1. INTRODUCTION

The degradation processes associated with loading–induced grain crushing and debonding affect the macroscopic mechanical behaviour of many natural geotechnical materials, such as pyroclastic weak rocks [1, 2], carbonate sands [3], calcarenites [4, 5] and compacted decomposed granite [6, 7].

In recent years, considerable efforts have been devoted to the mathematical development of constitutive elastoplastic models capable of reproducing the main aspects of the observed behaviour of these materials which are beyond the scope of classical Critical State elastoplastic models for soils [8–13]. These include: the occurrence of a peak in the stress–strain curve in a

*Correspondence to: Giulia M.B. Viggiani, Dipartimento di Ingegneria Civile, Università di Roma *Tor Vergata*, via del Politecnico 1, 00133 Roma, Italy
† E-mail: viggiani@uniroma2.it.

Received 14 January 2002
Revised 12 August 2002

contractant as well as in a dilatant regime [14, 1, 15]; the fact that the peak in the stress–strain curve does not correspond to the maximum rate of dilation [1, 4, 16, 14, 17]; the change of slope of the compressibility curve in one-dimensional and isotropic compression [18].

In addition to the well established features listed above, a recent experimental investigation of the mechanical behaviour of a pyroclastic weak rock has called into question the existence of a one-to-one stress–dilatancy relationship [2]; a similar feature was also observed by Cotecchia and Chandler [19] for a stiff natural clay deposit. In this paper we propose a model in which this effect is captured by allowing the friction angle of the material to decay with plastic straining in order to account for the effects of evolving grain size distribution.

The experimental motivation for our work stems from the results of a laboratory investigation of the mechanical behaviour of a pyroclastic deposit from Central Italy (*Pozzolana Nera*), which derives from the explosive activity of the volcanic complex of the Colli Albani near Rome. The material is a coarse-grained soft rock, whose physical properties and micro-structural features are described in detail in Reference [2]. Figure 1 shows the contact between two particles as observed by scanning electron microscopy, at a magnification factor of $1800\times$. Chemical micro-analyses of selected areas of the samples revealed that bonds are made of the same constituents of grains and therefore bond deterioration and grain crushing upon loading, which occur at relatively low stress levels (of the order of 50 kPa), are indistinguishable features of the mechanical behaviour.

As typical for geotechnical materials, the mechanical behaviour of intact *Pozzolana Nera* gradually changes from brittle and dilatant to ductile and contractant with increasing confining pressure. Figure 2 shows the stress–dilatancy relationships observed during drained triaxial compression in terms of dilatancy, d, as defined in (27) and stress ratio $\eta = q/p$, where the invariants p and q are defined in (1). The experimental stress–dilatancy relationships show that, at high confining stress, a peak of η occurs in a contractant regime ($d > 0$), while at low confining stress, in a dilatant regime ($d < 0$), the peak of η always precedes the point in the test where the

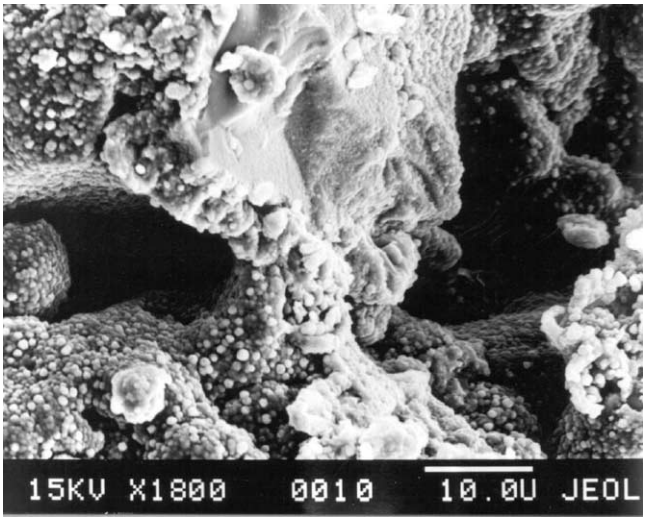

Figure 1. Micrograph of the contact between two particles of Pozzolana Nera.

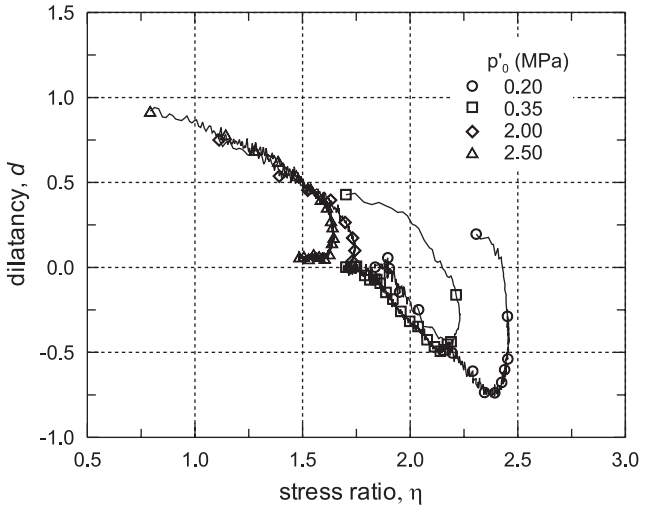

Figure 2. Experimental stress–dilatancy curves (adapted from Reference [2]).

dilatancy is minimum. The most striking feature of the experimental curves is that they are inconsistent with a one-to-one relationship between dilatancy and stress ratio. In particular, the condition $d = 0$, which in classical critical state models defines the friction of the material, is attained under different values of stress ratio. The hypothesis we make in the formulation of the model is that plastic straining induces a progressive reduction of the friction angle of the material. This is intuitively justified by the fact that grain crushing upon loading modifies the grading of the material and that finer granular materials exhibit lower friction angles [20, 21].

More specifically, we assume the existence of a virgin state for the intact material and of a fully degraded state for the material which has undergone grain crushing and debonding and interpolate between the two with the use of internal variables which evolve in the loading process. Each state is characterised by a one-to-one (e.g., linear) relationship between d and η while the d:η paths traced upon loading result from the material spanning with continuity different states. This may give rise to d:η relationships which are not one-to-one, see Figure 3.

Our relinquishing of the classical stress–dilatancy relationship has precedents. In order to model the effect of porosity on the volumetric behaviour of sands, Li and Dafalias [22] postulate a dependence of d on both η and a state parameter measuring the distance of the actual state from an assumed critical state curve in the v:p plane (here v denotes the specific volume). To the best of our knowledge, however, our proposed model is the first instance in which a complex stress–dilatancy relationship emerges in the context of strain–hardening elastoplasticity as a signature of the evolution of the shape of the yield locus induced by the microstructural changes associated with grain crushing.

One of the internal variables in the model is used to describe a downward translation of the isotropic virgin compression line as the material degrades and the fine fraction of the soil increases. This effect was observed in carbonate sands by Coop [3] and, although there is no direct evidence of it in the data reported by Cecconi and Viggiani [2], it is not inconsistent with the observed behaviour of intact Pozzolana Nera.

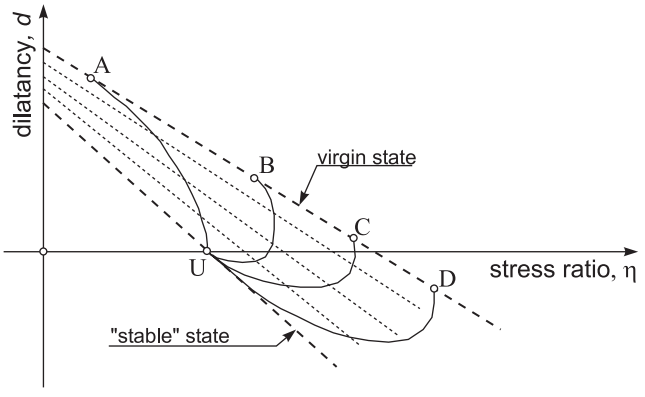

Figure 3. Conceptual sketch of stress–dilatancy relationships for evolving grain-size distribution.

With respect to other contributions to the modelling of loading induced structural changes in geomaterials, our work emphasizes the effects of grain crushing from the point of view of a phenomenological description based on strain–hardening elastoplasticity. Previous efforts within the same theoretical framework had focussed primarily on the effects of debonding in cemented soils, see e.g. [5]. Thus, we focus exclusively on grain crushing. Our model, however, has a very similar mathematical structure to that of [5], so that inclusion of the effects of debonding is straightforward through the addition of further internal variables, and it will be the subject of future work. On the other hand, a conspicuous body of literature addresses loading induced particle breakage phenomena in granular materials from a microscopic viewpoint, see, e.g., [23–28]. In addition, micro-mechanically based continuum models have recently been proposed, see, e.g., [29, 30]. With respect to all these papers, the major element of novelty of our analysis consists in the central role played by experimental measurements of stress–dilatancy data, and in our critical view towards the existence of a one-to-one stress–dilatancy relation.

The rest of the paper is organised as follows. Section 2 details the constitutive equations adopted in the formulation of the model. In Section 3 we illustrate the behaviour encoded in the model by means of three series of numerical simulations of single-element tests. In each series of tests, only one of the material parameters is varied, while the others are kept fixed, in order to highlight their individual influence. In Section 4 we discuss the application of our model to intact Pozzolana Nera. Here, the comparison of model predictions with the available experimental evidence is used mainly as a tool to assign a physically plausible set of mutually consistent constitutive parameters. A full geotechnical characterization of the mechanical behaviour of this material is beyond the scope of the present work. We believe that, in fact, such an endeavour is premature before further experimental work will have clarified important aspects of the material behaviour such as the role played by strain localization, as discussed in Reference [2]. The emphasis of this paper is on the qualitative features of material response in the presence of grain crushing, rather than on quantitative details peculiar to a specific material.

Finally, a few words on notation. Throughout the paper, the stress tensor and all the related quantities are effective stresses as defined by Terzaghi, unless otherwise stated. The usual sign convention of soil mechanics (compression positive) is adopted throughout. Both direct and index notations will be used to represent vector and tensor quantities according to convenience.

Following standard notation, for any two vectors $\mathbf{v}, \mathbf{w} \in \mathbb{R}^3$, the dot product is defined as $\mathbf{v} \cdot \mathbf{w} := v_i w_i$, and the dyadic product as: $[\mathbf{v} \otimes \mathbf{w}]_{ij} := v_i w_j$. Similarly, for any two second-order tensors $\mathbf{X}, \mathbf{Y} \in \mathbb{L}$, $\mathbf{X} \cdot \mathbf{Y} := X_{ij} Y_{ij}$ and $[\mathbf{X} \otimes \mathbf{Y}]_{ijkl} := X_{ij} Y_{kl}$. The quantity $\|\mathbf{X}\| := \sqrt{\mathbf{X} \cdot \mathbf{X}}$ denotes the Euclidean norm of $\mathbf{X}$.

In the representation of stress and strain states, use will sometimes be made of the following invariant quantities:

$$p := \frac{1}{3}\mathrm{tr}(\boldsymbol{\sigma}); \quad q := \sqrt{\frac{3}{2}}\|\mathbf{s}\|; \qquad \sin(3\theta) := \sqrt{6}\,\frac{\mathrm{tr}(\mathbf{s}^3)}{[\mathrm{tr}(\mathbf{s}^2)]^{3/2}} \tag{1}$$

where $\mathbf{s} := \boldsymbol{\sigma} - (1/3)\mathrm{tr}(\boldsymbol{\sigma})$ is the deviatoric part of the stress tensor, and

$$\varepsilon_v := \boldsymbol{\varepsilon} \cdot \mathbf{1}; \quad \varepsilon_s := \sqrt{\frac{2}{3}}\|\mathbf{e}\|; \quad \dot{\varepsilon}_v := \dot{\boldsymbol{\varepsilon}} \cdot \mathbf{1}; \qquad \dot{\varepsilon}_s := \sqrt{\frac{2}{3}}\|\dot{\mathbf{e}}\| \tag{2}$$

where $\mathbf{e} := \boldsymbol{\varepsilon} - (1/3)\mathrm{tr}(\boldsymbol{\varepsilon})$ and $\dot{\mathbf{e}} := \dot{\boldsymbol{\varepsilon}} - (1/3)\mathrm{tr}(\dot{\boldsymbol{\varepsilon}})$, are the deviatoric parts of the strain and the strain rate tensors, respectively.

2. CONSTITUTIVE EQUATIONS

2.1. Fundamental assumptions and evolution equations

In the following, attention will be restricted to quasistatic, isothermal processes and linear kinematics. We postulate that the strain tensor $\boldsymbol{\varepsilon}$ can be additively decomposed into an *elastic*, reversible part, $\boldsymbol{\varepsilon}^{\mathrm{e}}$ and a *plastic*, irreversible part $\boldsymbol{\varepsilon}^{\mathrm{p}}$, according to:

$$\boldsymbol{\varepsilon} = \boldsymbol{\varepsilon}^{\mathrm{e}} + \boldsymbol{\varepsilon}^{\mathrm{p}} \tag{3}$$

The current state of the material is described in terms of the effective stress tensor $\boldsymbol{\sigma}$ and a set of internal (hardening) variables $\mathbf{q}$, which describe the effects of the past loading history of the material. The evolution of the internal variables is associated to the macroscopically observable effects of the irreversible modifications in the microstructure—such as particle rearrangement or grain crushing—and is therefore linked to permanent deformations of the solid skeleton.

Based on the available experimental evidence—see, e.g., Reference [2]—in the development of the present theory it is assumed that *all* the mechanical effects of grain crushing can be accounted for through the introduction of suitable internal variables, the nature of which is to be defined according to the available knowledge of the influence of grain-size distribution on the behaviour of granular materials. This implies that grain crushing has no effects on the elastic behaviour of the material and rules out any form of elastoplastic coupling or damage.

In the framework of classical strain-hardening elastoplasticity, the evolution in time of stress and internal variables is given by the following differential-algebraic system of index one, see, e.g., Reference [31]:

$$\dot{\boldsymbol{\sigma}} = \mathbf{D}^{\mathrm{e}}[\dot{\boldsymbol{\varepsilon}} - \dot{\boldsymbol{\varepsilon}}^{\mathrm{p}}] \tag{4}$$

$$\dot{\boldsymbol{\varepsilon}}^{\mathrm{p}} = \dot{\gamma}\mathbf{Q}(\boldsymbol{\sigma}, \mathbf{q}) \tag{5}$$

$$\dot{\mathbf{q}} = \dot{\gamma}\mathbf{h}(\boldsymbol{\sigma}, \mathbf{q}) \tag{6}$$

$$\dot{\gamma} \geqslant 0, \quad f(\boldsymbol{\sigma}, \mathbf{q}) \leqslant 0, \quad \dot{\gamma} f(\boldsymbol{\sigma}, \mathbf{q}) = 0 \tag{7}$$

Equation (4) expresses the elastic constitutive equation in rate form. In the following, it is assumed that the elastic response of the material can be defined in terms of a *stored energy function* $\psi = \psi(\boldsymbol{\varepsilon}^e)$, such that

$$\boldsymbol{\sigma} = \frac{\partial \psi}{\partial \boldsymbol{\varepsilon}^e}(\boldsymbol{\varepsilon}^e) \tag{8}$$

or, in rate form

$$\dot{\boldsymbol{\sigma}} = \mathbf{D}^e(\boldsymbol{\varepsilon}^e)\dot{\boldsymbol{\varepsilon}}^e, \quad \mathbf{D}^e := \frac{\partial^2 \psi}{\partial \boldsymbol{\varepsilon}^e \otimes \partial \boldsymbol{\varepsilon}^e} \tag{9}$$

where $\mathbf{D}^e$ is the elastic tangent stiffness tensor. Irreversibility is introduced by postulating that, in any mechanical process, the stress is constrained to lie in the convex set $\mathbb{E}_\sigma$, defined through a suitable *yield function* $f(\boldsymbol{\sigma}, \mathbf{q})$, as

$$\mathbb{E}_\sigma := \{(\boldsymbol{\sigma}, \mathbf{q}) \mid f(\boldsymbol{\sigma}, \mathbf{q}) \leqslant 0\} \tag{10}$$

The boundary of $\mathbb{E}_\sigma$:

$$\partial \mathbb{E}_\sigma := \{(\boldsymbol{\sigma}, \mathbf{q}) \mid f(\boldsymbol{\sigma}, \mathbf{q}) = 0\} \tag{11}$$

represents the *yield surface* in stress space.

The evolution equations for the plastic strain tensor and for the internal variables are provided by the so-called *flow rule*, Equation (5), and *hardening law*, Equation (6). The symmetric, second-order tensor function $\mathbf{Q}(\boldsymbol{\sigma}, \mathbf{q})$ appearing in Equation (5) provides the plastic flow direction, while the hardening function $\mathbf{h}(\boldsymbol{\sigma}, \mathbf{q})$ specifies the type of hardening.

The (non-negative) scalar quantity $\dot{\gamma}$ appearing in Equations (5) and (6) is defined *plastic multiplier*, and is assumed to obey the so-called *Kuhn–Tucker complementarity conditions* given by Equations (7). These essentially define the loading/unloading conditions, by stating that plastic deformations may occur only when the stress state is on the yield surface. In addition to Equations (7), the plastic multiplier must satisfy the following *consistency condition*:

$$\dot{\gamma}\dot{f}(\boldsymbol{\sigma}, \mathbf{q}) = 0 \tag{12}$$

according to which, whenever plastic loading occurs ($\dot{\gamma} > 0$), the state of the material must remain on the yield surface.

An explicit expression for the plastic multiplier in terms of the strain rate is obtained from the consistency condition (12) as follows. If the current state of the material is on the yield surface ($f = 0$), constraint $(7)_2$ implies that

$$\dot{f} = \frac{\partial f}{\partial \boldsymbol{\sigma}} \cdot \mathbf{D}^e \dot{\boldsymbol{\varepsilon}} - \dot{\gamma}\left(\frac{\partial f}{\partial \boldsymbol{\sigma}} \cdot \mathbf{D}^e \mathbf{Q} - \frac{\partial f}{\partial \mathbf{q}} \cdot \mathbf{h}\right) \leqslant 0 \tag{13}$$

Assuming that, for all admissible states, the yield condition, the flow rule and the hardening law are such that

$$K_p := \frac{\partial f}{\partial \boldsymbol{\sigma}} \cdot \mathbf{D}^e \mathbf{Q} - \frac{\partial f}{\partial \mathbf{q}} \cdot \mathbf{h} > 0 \tag{14}$$

then, Equation (12) yields the equivalence:

$$\dot{f} = 0 \;\Leftrightarrow\; \dot{\gamma} = \frac{1}{K_p}\left\langle \frac{\partial f}{\partial \boldsymbol{\sigma}} \cdot \mathbf{D}^e \dot{\boldsymbol{\varepsilon}} \right\rangle \tag{15}$$

where $\langle x \rangle := (x + |x|)/2$ is the ramp function.

In the following developments, to keep the theory to an acceptable level of simplicity to be used in practical applications, we will assume that material behaviour is *isotropic*. Therefore, all the internal variables appearing in the vector $\mathbf{q}$ are scalar quantities, and the constitutive functions ψ, f and g can be expressed in terms of any complete set of invariants of their tensorial arguments.

2.2. Stored energy function and elastic behaviour

The stored energy function adopted in the development of the constitutive model is defined by the following two-invariant expression:

$$\psi(\varepsilon_v^e, \varepsilon_s^e) = \tilde{\psi}(\varepsilon_v^e) + \frac{3}{2} G_0 (\varepsilon_s^e)^2 \tag{16}$$

where:

$$\tilde{\psi}(\varepsilon_v^e) := \begin{cases} \hat{\kappa} p_r \exp(\varepsilon_v^e/\hat{\kappa} - 1) & (\varepsilon_v^e \geqslant \hat{\kappa}) \\ p_r \varepsilon_v^e + p_r (\varepsilon_v^e - \hat{\kappa})^2/(2\hat{\kappa}) & (\varepsilon_v^e < \hat{\kappa}) \end{cases} \tag{17}$$

the parameter p_r is a reference mean stress (e.g. 100 kPa), and $\hat{\kappa}$, G_0 and α are material constants.

According to Equation (17), for $\varepsilon_v^e \geqslant \hat{\kappa}$ the free energy function (16) describes a pressure-dependent, hyperelastic behaviour, with a constant shear modulus G_0 and a bulk modulus $K = p/\hat{\kappa}$. For $\varepsilon_v^e < \hat{\kappa}$, the stored energy function reduces to the classical quadratic expression of linear elasticity. Equation (16) is a simplified version of the stored energy function proposed by Houlsby, see e.g., Reference [32]. The minor modification introduced with the switch condition (17) allows to extend the validity of the original model to the tensile stress range.

2.3. Yield function

After an original proposal of Lagioia *et al.* [33], the following expression is assumed for the yield function f:

$$f(p, q, \theta, p_s, b, m, M) = A^{K_1/C} B^{-K_2/C} p - b p_s \tag{18}$$

where

$$K_1(m) := \frac{m(1-a)}{2(1-m)} \left\{ 1 + \sqrt{1 - \frac{4a(1-m)}{m(1-a)^2}} \right\} \tag{19}$$

$$K_2(m) := \frac{m(1-a)}{2(1-m)} \left\{ 1 - \sqrt{1 - \frac{4a(1-m)}{m(1-a)^2}} \right\} \tag{20}$$

$$A(p, q, \theta, m, M) := 1 + \frac{1}{K_1(m)\mu(\theta, M)} \frac{q}{p} \tag{21}$$

$$B(p, q, \theta, m, M) := 1 + \frac{1}{K_2(m)\mu(\theta, M)} \frac{q}{p} \tag{22}$$

$$C(m) := (1 - m)(K_1 - K_2) \tag{23}$$

$$\mu(\theta, M) := c_1 [1 + c_2 \sin(3\theta)]^n M \tag{24}$$

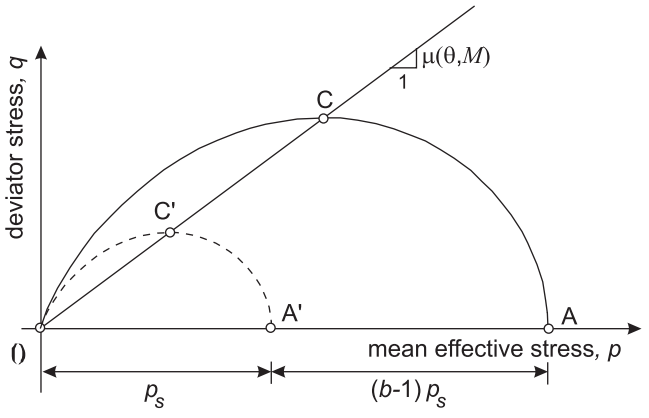

Figure 4. Yield surface in q:p plane, for $\theta = \text{const.}$.

A section of the yield surface ($f = 0$) in a $\theta = \text{const.}$ plane is shown in Figure 4. In Equation (18), a, c_1, c_2 and n are material constants. The first controls the shape of the yield surface close to the isotropic axis (see [33]), the others control the dependence of parameter μ on Lode angle θ, according to a general expression first proposed by van Eekelen [34]. The quantities c_1 and c_2 can be expressed as functions of the ratio $c_M := \mu_e/\mu_c$ between the values taken by the function $\mu(\theta, M)$ in axisymmetric extension ($\theta = -\pi/6$) and axisymmetric compression ($\theta = \pi/6$):

$$c_1 := \frac{1}{2^n}[1 + (c_M)^{1/n}]^n, \quad c_2 := \frac{1 - (c_M)^{1/n}}{1 + (c_M)^{1/n}} \tag{25}$$

The effect of loading history is described by the following set of internal variables:

$$\mathbf{q} \equiv \{p_s \;\; b \;\; M \;\; m\}^{\mathrm{T}} \tag{26}$$

The product $b\,p_s$ represents the p-co-ordinate of point A, at the intersection of the yield surface and the isotropic axis (see Figure 4), and controls the size of the elastic domain. For $b = \text{const.}$, the variable p_s plays the role of the preconsolidation pressure, as in classical critical-state models. In an isotropic compression path starting from an isotropic, plastic state, as p_s changes with plastic strain, the state of the material describes a *virgin compression curve* in the ε_v:p plane, whose position depends on the actual value of b. In Reference [9], the variable $b \geqslant 1$ is introduced to account for the mechanical effects of interparticle bonding, which are modelled as a net increase in the size of the yield surface, as compared to that of the unbonded material (the dotted curve OC'A' in Figure 4). Here the same internal variable is introduced to account for a different physical phenomenon, namely, the translation of the isotropic virgin compression curve as the grain-size distribution is changed, see Section 3.1.

According to Equations (18), (24), M represents the stress ratio q_C/p_C at point C, where $\partial f/\partial p = 0$ on the yield surface (see Figure 4), for $\theta = \pi/6$ (axisymmetric compression). Through function μ, which specifies the dependence of this quantity on the Lode angle, M controls the aspect ratio of all the θ-sections of the yield locus, and hence the stress ratio at failure (i.e., the mobilized friction angle) for general stress states. In classical critical state models, as well as in other more recent formulations for isotropic materials—see, e.g., References [35, 36]—this quantity is taken to be constant. Here, however, its evolution with

plastic strains is introduced in order to account for the effects of changes in grain-size distribution on the critical friction angle of the material, as observed, e.g., in References [20, 21].

As discussed in Reference [33], parameter m controls the shape of the yield surface for a given aspect ratio. This has a strong impact on the plastic flow direction, and in particular on the relation between dilatancy d, defined as

$$d \coloneqq \frac{\dot{\varepsilon}_v^{\mathrm{p}}}{\dot{\varepsilon}_s^{\mathrm{p}}} \tag{27}$$

and the stress ratio $\eta \coloneqq q/p$, as it will be clarified in the following section.

2.4. Flow rule

To specify the flow rule for plastic strain rates, the assumption is made here that the plastic flow direction is *associated* with the yield surface in the deviatoric plane, while it might be *non-associated* in the θ-sections of the yield locus with planes containing the isotropic axis. As proposed, e.g. by Runesson [37], this can be obtained by setting:

$$\mathbf{Q}(\boldsymbol{\sigma}, \mathbf{q}) \coloneqq \mathbf{N}(\boldsymbol{\sigma}, \mathbf{q}) \frac{\partial f}{\partial \boldsymbol{\sigma}}(\boldsymbol{\sigma}, \mathbf{q}) \tag{28}$$

where

$$\mathbf{N}(\boldsymbol{\sigma}, \mathbf{q}) \coloneqq \mathbf{I} - \chi(\boldsymbol{\sigma}, \mathbf{q}) \mathbf{1} \otimes \mathbf{1} \tag{29}$$

is a fourth-order non-associativeness tensor. The scalar χ may be, in general, state dependent. However, to keep the formulation of the model as simple as possible, in the following it will be assumed, as in Reference [38], that

$$\chi = \frac{\beta}{3(1+\beta)} \tag{30}$$

and $\beta = \text{const}$. Full associativity is recovered when $\beta = 0$.

According to Equations (28) and (29), the first two invariants of the plastic strain rate are given by:

$$\dot{\varepsilon}_v^{\mathrm{p}} = \mathrm{tr}(\dot{\boldsymbol{\varepsilon}}^{\mathrm{p}}) = \dot{\gamma}(1 - 3\chi)\mathrm{tr}\left(\frac{\partial f}{\partial \boldsymbol{\sigma}}\right) \tag{31}$$

$$\dot{\varepsilon}_s^{\mathrm{p}} = \sqrt{\frac{2}{3}} \|\dot{\mathbf{e}}^{\mathrm{p}}\| = \dot{\gamma}\sqrt{\frac{2}{3}} \left\| \mathrm{dev}\left(\frac{\partial f}{\partial \boldsymbol{\sigma}}\right) \right\| \tag{32}$$

In the particular case of $\theta = \text{const.} = \pi/6$, the above expressions and eq. (18) yield:

$$\dot{\varepsilon}_v^{\mathrm{p}} = \dot{\gamma}(1 - 3\chi)\frac{\partial f}{\partial p} \tag{33}$$

$$\dot{\varepsilon}_s^{\mathrm{p}} = \dot{\gamma}\frac{\partial f}{\partial q} \tag{34}$$

The dilatancy in axisymmetric compression is then given by

$$d(\eta, m, M) = (1 - 3\chi)m[M - \eta]\left[1 + \frac{aM}{\eta}\right] \tag{35}$$

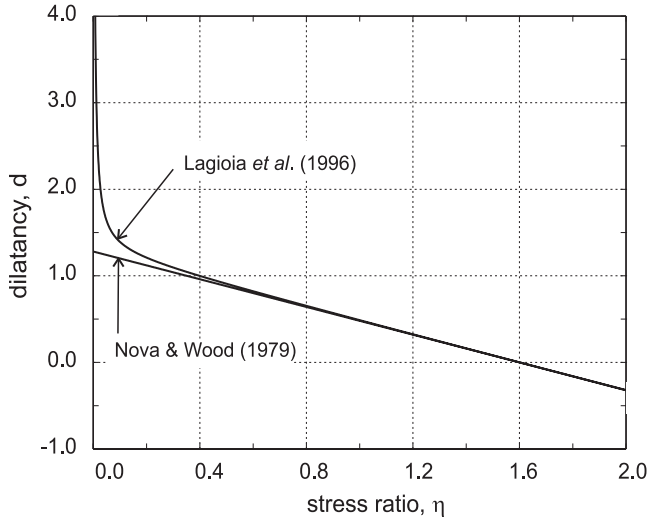

Figure 5. Stress ratio–dilatancy curves for the plastic potentials of Lagioia *et al.* [33] and Nova and Wood [39] in axisymmetric compression, $\chi = 0$, $a = 0.01$, $M = 1.6$.

For $M = \text{const.}$ and $m = \text{const.}$, the above expression is identical to the stress ratio-dilatancy equation proposed by Lagioia *et al.* [33]:

$$d(\eta) = (1 - 3\chi)m[M - \eta]\left[1 + \frac{aM}{\eta}\right] \quad (m, M = \text{const.}) \tag{36}$$

which for $a = 0$ reduces further to the dilatancy equation first proposed by Nova and Wood:

$$d(\eta) = (1 - 3\chi)m[M - \eta] \quad (m, M = \text{const.}) \tag{37}$$

Equations (36) and (37) are plotted on the d:η plane in Figure 5. A detailed examination of the two expressions (36) and (37) above, and of the corresponding plots in Figure 5, shows that M is the intercept of the $d(\eta)$ curve with the η-axis, while m defines the slope of the $d(\eta)$ curve at high stress ratios (i.e., when the yield point is located around or left of point C in Figure 4). In the present model, both these quantities are allowed to vary with plastic strain, to reflect the changes in grain size distribution induced by grain crushing.

2.5. Hardening laws

The formulation of the constitutive equations is completed by specifying the evolution laws for the four internal variables p_s, b, M and m, the physical meaning of which has been discussed in Section 2.3. A possible choice for the hardening laws inspired by the work of Nova and coworkers, see, e.g. References [40, 39, 9], is the following:

$$\dot{p}_s = \rho_s p_s(\dot{\varepsilon}_v^{\mathrm{p}} + \xi_s \dot{\varepsilon}_s^{\mathrm{p}}) \tag{38}$$

$$\dot{b} = -\rho_b(b - 1)(|\dot{\varepsilon}_v^{\mathrm{p}}| + \xi_b \dot{\varepsilon}_s^{\mathrm{p}}) \tag{39}$$

$$\dot{M} = -\rho_M(M - M_{\mathrm{crit}})(|\dot{\varepsilon}_v^{\mathrm{p}}| + \xi_M \dot{\varepsilon}_s^{\mathrm{p}}) \tag{40}$$

$$\dot{m} = -\rho_m(m - m_{\text{crit}})(|\dot{\varepsilon}_v^{\text{p}}| + \xi_m \dot{\varepsilon}_s^{\text{p}}) \tag{41}$$

which correspond to the following expression for the hardening function $\mathbf{h}$ in Equation (6):

$$\mathbf{h} = \begin{Bmatrix} \rho_s p_s(\hat{T} + \xi_s \hat{N}) \\ -\rho_b(b-1)(|\hat{T}| + \xi_b \hat{N}) \\ -\rho_M(M - M_{\text{crit}})(|\hat{T}| + \xi_M \hat{N}) \\ -\rho_m(m - m_{\text{crit}})(|\hat{T}| + \xi_m \hat{N}) \end{Bmatrix} \tag{42}$$

where ρ_s, ξ_s, ρ_b, ξ_b, ρ_M, ξ_M, M_{crit}, ρ_m, ξ_m, and m_{crit} are material constants, and

$$\hat{T} \coloneqq \text{tr}(\mathbf{Q}), \quad \hat{N} \coloneqq \sqrt{\frac{2}{3}}\|\text{dev}(\mathbf{Q})\| \tag{43}$$

are the volumetric and deviatoric components of the plastic flow direction tensor $\mathbf{Q}$.

According to Equations (38)–(41), the evolution of the internal variables is linked to both the volumetric and the deviatoric components of plastic strain rates. Equation (38) coincides with the expression first proposed by Nova in Reference [40], and reduces to the classical exponential relation between the preconsolidation pressure p_s and the plastic volumetric strain of Critical State Soil Mechanics, when distortional hardening is excluded ($\xi_s = 0$). Equation (39) is similar to the one proposed by Gens and Nova [9] to describe the mechanical degradation of interparticle bonding in ''structured'' granular soils. Here, the physical meaning is different, in that this evolution equation is introduced to account for the phenomenological effects of grain crushing. To the same end we have introduced also the two (new) hardening laws (40), (41), motivated by the following qualitative considerations.

Available experimental evidence suggests that, for granular materials with permanent grains, the ultimate value of the friction angle at constant volume is an increasing function of the mean grain diameter (see, e.g., References [20, 21]). Moreover, it has also been observed that the position of the virgin compression line (VCL), in the ε_v: ln(p) plane, may depend on the mean grain diameter. Indeed, for carbonate sands, Coop [9] has reported that increasing the fine fraction of the soil produces a downward shift of the VCL. Finally, it is also likely that the grain size distribution might affect the overall shape of the yield locus, although, to the authors knowledge, no conclusive quantitative evidence exists in the literature concerning this last point.

The above considerations can provide useful indications on the nature of the internal variables to be taken into account to describe the effects of grain crushing and how their evolution equations should be constructed. As detailed in Section 2.3, the position of the VCL in the ε_v: ln(p) plane is controlled by variable b, while the ultimate friction angle and the shape of the yield locus are associated to M and m, respectively.

A micromechanically based strategy to construct the appropriate evolution equations for b, M and m, similar in spirit to the one actually pursued in References [29, 30], would entail:

(i) assigning a relationship between b, M, and m and some relevant quantitative descriptors of the grain size distribution (e.g. mean grain diameter, coefficient of uniformity, etc.);
(ii) providing an evolution law linking the changes in grain size distribution parameters and the associated plastic strain rate, based, e.g. on consideration on the energy dissipated in the grain crushing process.

In lack of sufficient experimental data, we take instead a phenomenological viewpoint, i.e. we formulate the evolution equation directly at the macroscopic level, as in eqs. (39)–(41).

It is worth noting that Equations (39)–(41) imply a monotonic evolution of b, M, m towards the asymptotic values

$$b = 1, \quad M = M_{\text{crit}}, \quad m = m_{\text{crit}} \tag{44}$$

describing a material with a stable grain size distribution. This may be intuitively justified from the observations by Fuller and Thompson [41] that grain crushing gradually comes to an end as the shape of the grain size distribution approaches a stable curve known as *Fuller curve*. An indication of the existence of a stable grain size distribution reached after high-pressure one-dimensional compression of sands and glass beads can be found in Reference [25]. Moreover, lesser changes of grading with increasing applied load are observed in the experiments in References [26, 29, 27]. Ultimately, however, the existence of steady asymptotic values for b, M, and m should be regarded as a physically plausible working hypothesis. A quantitative critical assessment of its range of validity deserves further study, and is the subject of current research.

Parameters ρ_b, ρ_M, and ρ_m control the speed at which, for a given plastic strain history, the asymptotic state is reached. Parameters ξ_b, ξ_M, and ξ_m measure the influence of the deviatoric component of the plastic strain rate in the evolution process. The influence of these constants on predicted material behaviour is discussed in the following section.

3. QUALITATIVE RESPONSE OF THE MODEL

In this section, the results of a series of numerical simulations of single-element tests are presented in order to assess, from a qualitative point of view, the effects of the proposed approach to the modelling of grain crushing on predicted material response. The procedure adopted for the numerical integration of the constitutive equations along the prescribed loading paths is a modified version of an algorithm initially proposed by Bardet and Choucair [42], and is detailed in the appendix.

In the simulations, it has been assumed that the internal variables M and m are linked by the following additional condition:

$$Mm = d_0 = \text{const.} \tag{45}$$

The rationale for this choice will be clarified in Section 4, with reference to the observed behaviour of Pozzolana Nera. Hypothesis (45) allows to remove variable m from the set of internal variables, and thus to eliminate ρ_m, ξ_m, m_{crit} from the set of material parameters required to characterize the behaviour of the material.

The complete set of numerical simulations is detailed in Table I, in terms of prescribed loading path, assumed initial state and assumed material parameters. Concerning this last point, three different sets of parameters have been selected for the simulations, all based on the model calibration for the Pozzolana Nera which is discussed in detail in the next Section 4. These are given in Table II. In each of the three sets, one of the parameters affecting material behaviour upon grain crushing (ρ_b, ρ_M, ξ_M) has been varied in the range indicated in the table, to highlight its influence on predicted material response.

Table I. Numerical testing program.

Test #	Test type	Parameter set (see Table II)	p_0 (kPa)	q_0 (kPa)	p_{s0} (kPa)	b_0	M_0
1–4	ISO	1	1000.0	0.0	3000.0	1.8	2.3
5–8	TX–CD	2	1404.0	0.0	2400.0	1.5	2.3
9–12	TX–CD	2	214.0	0.0	1800.0	1.5	2.3
13–16	TX–CU	3	799.0	0.0	3100.0	1.5	2.3

Note: ISO = isotropic compression test; TX–CD = drained axisymmetric compression test; TX–CU = isochoric axisymmetric compression test.

Table II. Material parameters adopted in the simulations of Section 3.

Parameter	Set #1 (ISO)	Set #2 (TX–CD)	Set#3 (TX–CU)
$\hat{\kappa}$	0.002	0.002	0.002
G_0 (kPa)	2.5×10^5	2.5×10^5	2.5×10^5
p_r (kPa)	400.0	400.0	400.0
M_{crit}	1.6	1.6	1.6
c_M	0.652	0.652	0.652
a	0.2	0.2	0.2
β	0.22	0.22	0.22
ρ_s	18.0	18.0	18.0
ξ_s	0.0	0.0	0.0
ρ_M	0.008	0.0–0.01	0,008
ξ_M	2.0×10^3	2.0×10^3	$0.0–1.0 \times 10^4$
ρ_b	5.0–40.0	6.0	6.0
ξ_b	0.25	0.25	0.25
d_0	2.07	2.07	2.07

3.1. Isotropic compression tests

A first group of numerical simulations refers to the model response under an isotropic compression path, starting from an initial isotropic state. Material parameters have been assigned as in set #1, Table II. Tests #1–4 differ only in the assumed values of parameter ρ_b, which range from 5.0 (test 1) to 40.0 (test 4). The results of the simulations are plotted in the v: log p plane in Figure 6. For comparison, the compression curve of an initially stable material (i.e. for which $b_0 = 1$) is also plotted in the figure.

All the predicted compression curves show an initially elastic behaviour, followed after yielding by an abrupt increase in compressibility. In the elastoplastic regime, the compression curves all show a more or less pronounced concavity upwards, which result from the softening process associated to the reduction in b. As expected from the assumed hardening law (39), this effect increases with ρ_b: the larger is ρ_b, the higher is the decrease in stiffness observed at yield. At large volumetric plastic strains, the value of b tends to $b_{\text{crit}} = 1$, and thus all the compression curves approach asymptotically the limit compression curve for the stable material, rapidly for high ρ_b values, slowly for low ρ_b values.

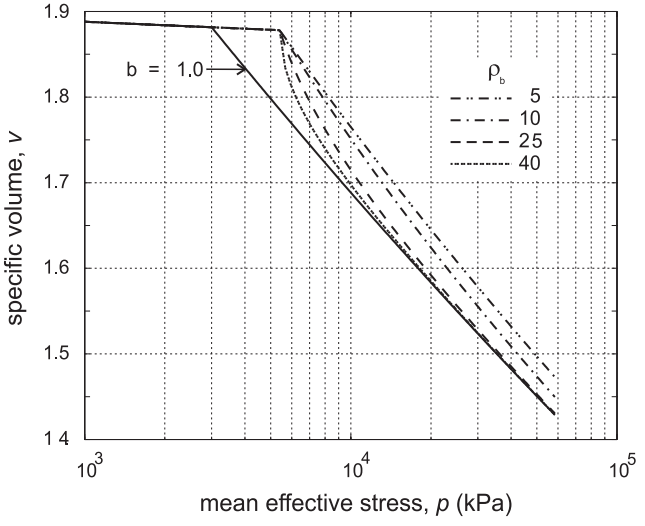

Figure 6. Results of isotropic compression tests #1–4.

This behaviour is qualitatively very similar to the response in isotropic (or one-dimensional) compression of 'structured' clays [18] or of cemented sands [5]. However, rather than describing the reduction in yield stress associated to the loss of interparticle bonds, the intention here is to model a gradual downward shift of the virgin compression line as the grain size distribution of the soil is modified by grain crushing, with an increase of the fine fraction. Such a downward shift has been reported by [3] in an uncemented carbonate sand for which the initial grading had been subsequently modified by increasing the proportion of fines. Experimental evidence of a compression curve similar to Figure 6 in an uncemented sand can be found in References [25, 28], where it is attributed to breakage of particle asperities upon loading.

It is worth emphasising that the monotonic reduction in b implied by the hardening law (39) does not always produce a decrease in the distance between the current yield locus and the yield locus of the corresponding stable material, measured by the quantity $p_m := (b-1)\,p_s$. In fact

$$\dot{p}_m = \dot{b}\,p_s + (b-1)\dot{p}_s \tag{46}$$

and while the first term on the right hand side is always negative, the second is always positive due to volumetric hardening, and might be larger than the first for particular combinations of the initial state and the material parameters ρ_s and ρ_b. This is demonstrated by the data in Figure 7, where the values of p_m computed for each tests are plotted as a function of the volumetric strain. This type behaviour would be inconsistent with destructuration processes associated solely to the breakage of interparticle bonds.

3.2. Axisymmetric compression tests

To investigate the influence of parameters ρ_M and ξ_M on the predicted material response two different series of axisymmetric compression tests have been performed considering different initial states and loading conditions.

In the first series of tests (tests #5–12), the material is loaded in drained conditions, keeping the radial stress constant while the axial strain is increased at a constant rate (TX–CD path).

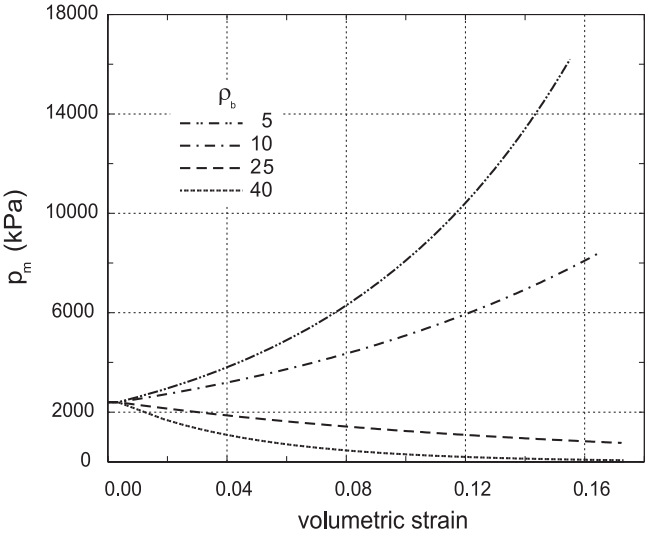

Figure 7. Isotropic compression tests: effect of parameter ρ_b.

Material parameters have been assigned as in set #2, Table II. In tests #5–8, the initial (isotropic) stress state is relatively close to the initial yield locus, so that the volumetric behaviour at yield is contractant; in tests #9–12, on the contrary, the initial stress state is highly overconsolidated[†], and the volumetric response at yield is dilatant.

Computed results from tests #5–8 are plotted, in the q:ε_s and ε_v:ε_s planes, in Figure 8, and in the η:d plane in Figure 10a. For $\rho_M = 0.0$, M remains constant, and the predicted behaviour is similar to that of classical isotropic-hardening elastoplastic models for soils (see, e.g., References [39, 36]). In particular, the stress–strain curve shows a monotonic increase in the deviatoric stress up to a limit condition at very large strains. This ductile behaviour is due to the monotonic increase of p_s implied by Equation (38), which, for $\xi_s = 0.0$, leads to a ultimate critical state condition when $\dot{\varepsilon}_v^{\mathrm{p}} = 0$. However, as ρ_M increases up to 0.01 (tests #5–8), a dramatic change in the material response is observed. In fact, with increasing volumetric and deviatoric components of plastic strain, M is reduced from its relatively large initial value to the much lower final asymptotic value $M_{\mathrm{crit}} = 1.6$, which represents the stress ratio at the ultimate limit state. This process occurs gradually, so that the stress–strain curve may show a peak in the deviatoric stress, when the competing effects of volumetric hardening on p_s and grain crushing-induced softening on M are such that the resulting value of the plastic modulus is zero. The actual value of the deviatoric stress at peak strongly depends on the assumed values of ρ_M, as clearly indicated by the data in Figure 8(a).

As any change in M—and thus in m, according to Equation (45)—has also an effect on the shape of the yield locus, the assumed value of ρ_M has also a strong impact on the volumetric response of the material and on its stress–dilatancy relationship, as shown in Figures 8(b) and 10(a). In this respect, it is worth noting that, while in a classical critical state model with

[†] For an initial isotropic stress state $\boldsymbol{\sigma} = p_0\mathbf{1}$, the overconsolidation ratio can be defined as $R := b\,p_s/p_0$.

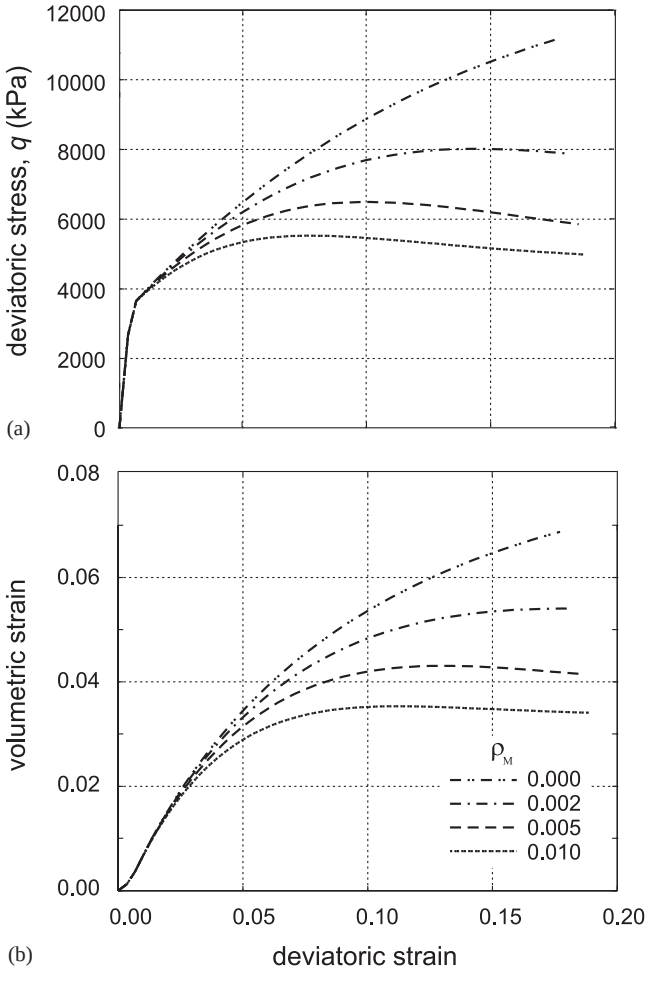

Figure 8. Results of drained triaxial compression tests #5–8.

isotropic hardening (i.e., with $\xi_s = 0$) an initially contractant material reaches its maximum stress ratio at $d = 0$ and cannot experience any dilatant behaviour, the proposed formulation is capable of reproducing a response in which an initially contractant material may eventually become dilatant before reaching the ultimate critical state and, contrary to the predictions of classical stress–dilatancy relationships (see, e.g. [43, 44, 40]), the peak stress ratio does not correspond to a minimum of d. This is clearly demonstrated by the η:d curves for tests #6 and 7, with $\rho_M = 0.005$ and 0.01, respectively.

Figures 9 and 10(b) show the computed results from tests #9 to #12, referring to an initially heavily overconsolidated soil. In all these tests, the stress–strain curves show a well defined peak of the deviator stress, corresponding to the first yield point, followed by a relatively fast decay of the deviatoric stress as plastic strain is increased, while the volumetric response is characterized by a strongly dilatant behaviour. However, while in test #9, with $\rho_M = 0$, the maximum stress ratio corresponds to the minimum value of the dilatancy d, in agreement with the stress–

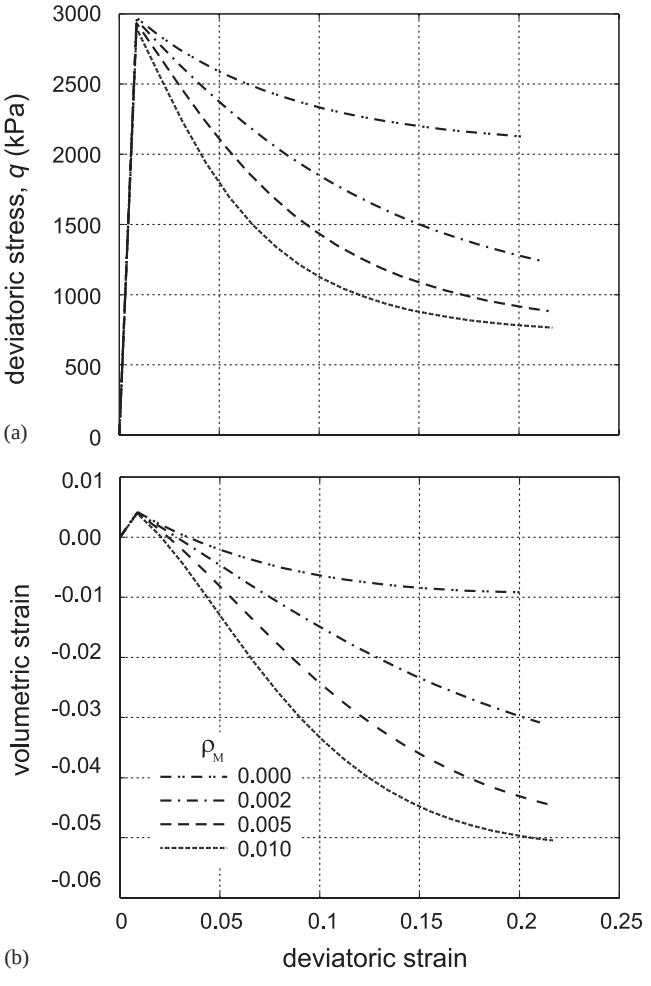

Figure 9. Results of drained triaxial compression tests #9–12.

dilatancy relation (36), this is no longer true when ρ_M is increased. In fact, in both tests #11 ($\rho_M = 0.005$) and #12 ($\rho_M = 0.01$) the peak of η occurs before the minimum value of dilatancy is reached. The general picture of the predicted stress–dilatancy curves shown in Figure 10 closely resembles the experimental observations for *Pozzolana Nera* reported by Cecconi and Viggiani [2] (Figure 2) and the qualitative pattern illustrated in Figure 3.

In the last series of tests (tests #13–16), the material is loaded in isochoric conditions by prescribing a radial strain rate equal to half the axial strain rate (TX–CU path). Material parameters have been specified as in set #3, Table II. The results of the numerical simulations are shown in Figure 11, in the $q{:}\varepsilon_s$ and $q{:}p$ planes, respectively. The pattern of the observed behaviour is similar in all four tests: after first yield, the deviator stress continues to increase with only a minor reduction in the overall stiffness until a peak is reached when the stress path approaches the line of zero-dilation. At this point, the only changes in the size of the yield locus

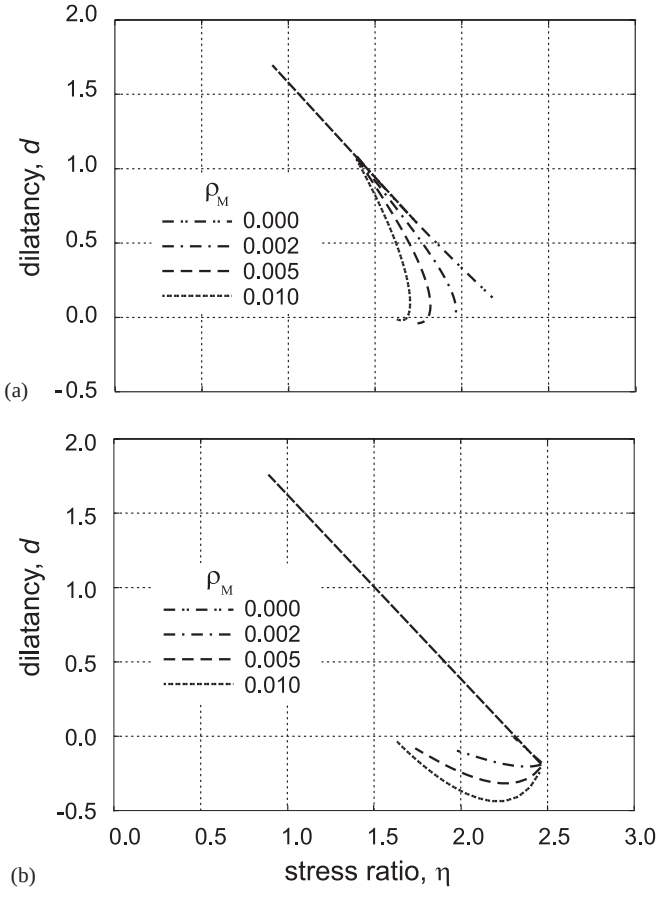

Figure 10. Stress–dilatancy curves: (a) tests #5–8; (b) tests #9–12.

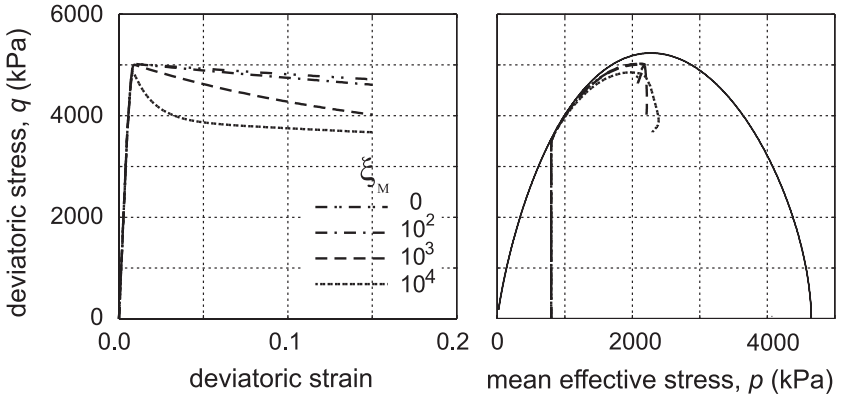

Figure 11. Results of isochoric triaxial compression tests #13–16.

are due to the gradual reduction in M associated with irreversible deformations. However, large quantitative differences in both the stress–strain curves and the stress paths are apparent as ξ_M changes between 0.0 and 1.0×10^4. This is because ξ_M controls the rate of reduction of M with the plastic deviatoric strain rate: the higher ξ_M, the larger the influence of plastic distortions on the assumed macroscopic effects of grain crushing. In an isochoric loading path, the plastic and elastic volumetric strain rates are such that $|\dot{\varepsilon}_v^{\mathrm{p}}| = |\dot{\varepsilon}_v^{\mathrm{e}}|$, and since $|\dot{\varepsilon}_v^{\mathrm{e}}|$ is usually small due to the relatively high elastic bulk stiffness of the material, so is the plastic volumetric strain rate. Therefore, when ξ_M is small (or zero) and the soil is deformed at constant volume, only a limited change in both M and m can occur, and the predicted response of the model is rather insensitive to the assumed value of ρ_M, not differing much from that of a classical isotropic hardening elastoplastic model. A consequence of this observation is that an accurate experimental determination of the parameters ρ_M and ξ_M requires data from both drained and undrained tests, in order to correctly quantify the influence of the volumetric and deviatoric components of plastic strains on grain crushing.

4. APPLICATION TO POZZOLANA NERA

In order to test the capability of the model to reproduce the observed behaviour of natural materials, we now consider its application to *Pozzolana Nera* [2,45]. In the calibration of material parameters we pursue two different strategies. First we explore the possibility of finding a reasonable agreement with the available experimental evidence within the framework of associative elastoplasticity. The identification of the plastic potential with the yield surface allows in this case to infer directly the shape of the yield locus and its evolution during the loading process from the available dilatancy data. This also provides a way to assess the limits of applicability of associative plasticity to this class of materials. In the second step, we relax the assumption of normality to improve the quantitative agreement between predictions and observations.

The calibration of the model requires the evaluation of the following material parameters:

- $\hat{\kappa}$, G_0, p_r, which define the elastic behaviour of the material;
- M_{crit}, c_M, m_{crit}, a, which control the shape of the yield locus;
- β, which measures the deviation from normality in the $q{:}p$ plane;
- ρ_s, ξ_s, ρ_M, ξ_M, ρ_m, ξ_m, ρ_b, ξ_b, which control the hardening laws (38)–(42).

The procedures adopted in the determination of these parameters are detailed in Section 4.1 for the associative case, and in Section 4.2 for the non-associative case. The resulting numerical values are summarized in Table III.

4.1. Associative case

In the hypothesis of associative plastic flow, $\beta = 0$. As for the elastic parameters, $\hat{\kappa}$ has been determined from the unloading branch of the compression curves from one-dimensional compression tests. The shear modulus, G_0, has been obtained from the initial slope of the $q{:}\varepsilon_s$ curves from drained triaxial compression tests. Parameter p_r has been set by prescribing that the Poisson ratio is positive, and equal to 0.06 when $p \leqslant p_r$.

In the associative case, by definition, the yield function and the plastic potential coincide. Therefore, we can determine the values of M_{crit}, m_{crit}, and a from the dilatancy curves already

Table III. Material parameters for the Pozzolana Nera.

Parameter	Set #1 (Associative case)	Set #2 (Non-associative case)
$\hat{\kappa}$	0.002	0.002
G_0 (kPa)	2.5×10^5	2.5×10^5
p_r (kPa)	400.0	400.0
M_{crit}	1.6	1.6
c_M	0.652	0.652
a	0.001	0.2
β	0.0	0.22
ρ_s	18.0	18.0
ξ_s	0.0	0.0
ρ_M	0.008	0.008
ξ_M	2000.0	2000.0
ρ_b	6.0	6.0
ξ_b	0.25	0.25
d_0	2.07	2.07

shown in Figure 2. As it is apparent from the figure, all the curves tend to converge at the end of the tests towards a unique point on the η axis. The stress ratio at this point represents the critical value M_{crit}.

It would be tempting to deduce the critical value of the parameter m from the final portion of the dilatancy curves relative to the specimens tested at the lowest confining stresses, for which the experimental points fall close to a straight line. However, in the absence of direct evidence concerning the homogeneity of the deformation within the sample, and lacking direct experimental verification that grain crushing processes have come to an end, we refrain from attributing to this interpretation of the experimental data any significance beyond that of a convenient working hypothesis enabling us to fix, in the d:η plane, the dilatancy line corresponding to the fully degraded state.

Another important experimental observation from the data in Figure 2 is that the points corresponding to the first yield in each test fall approximately on a straight line. Moreover, the intersection point between this line and the fully degraded dilatancy line falls on the d axis, at $d = d_0 = 2.07$. Based on this observation, we slave the evolution law of m to the one of M by imposing that

$$Mm = d_0 = \text{const.} \tag{47}$$

With Equation (47), m is suppressed from the set of internal variables, so that the corresponding parameters ρ_m, ξ_m, m_{crit} are no longer needed and they do not appear in Table III.

Parameter c_M is determined by prescribing that the friction angle at critical state is the same in triaxial compression and extension. The characterization of the yield locus is completed by assigning parameter a. Since no experimental data are available concerning the stress–dilatancy relationship at low stress ratios, a direct estimate is not possible. We resort instead to the best fit of the experimental results, as detailed below.

As for the parameters entering the hardening laws, we begin by observing that $-\xi_s$ represents the dilatancy at an ultimate, limit state in which the hardening modulus vanishes. Therefore, the existence of a critical state requires that $\xi_s = 0$.

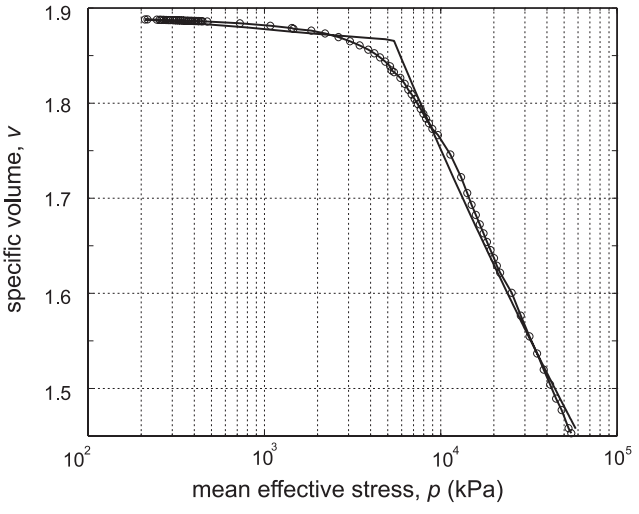

Figure 12. Isotropic compression test.

In a loading condition of purely isotropic compression, starting from an isotropic state, the material response is only determined by the parameters ρ_s and ρ_b. Therefore, experimental data from isotropic compression test can be used to estimate ρ_s and ρ_b by trial and error, through curve-fitting.

The remaining parameters, namely, ρ_M, ξ_M, ξ_b, and a, are evaluated by comparing predicted and observed responses along drained and undrained triaxial compression paths. As already remarked in Section 3.2, it is worth noting that a proper characterization of the parameters entering in the hardening laws cannot be obtained by considering the results from drained triaxial tests alone, since they do not provide sufficient indications concerning the relative importance of the deviatoric and volumetric components of plastic strain rate in the degradation process. The balance between these two components is weighted by parameters ξ_b and ξ_M, so that information on them can be deduced from the undrained tests, in which the degradation processes are mainly due to plastic distorsions.

Figures 12–15 illustrate the comparison between model predictions and observed behaviour. The numerical simulations require the assignment of the initial state of the material in terms of stress components and internal variables. Despite the fact that all specimens experienced the same geological history, significant variations in the microstructure of different specimens are to be expected, due to the observed small-scale heterogeneity of the Pozzolana Nera [45, 2]. Therefore, in the numerical simulations, the initial values of the internal variables have been estimated individually for each specimen to obtain the best fit of the experimental data, and are reported in Table IV.

The results from an isotropic compression test are shown in Figure 12. The model captures relatively well the trends of the experimental data in the fully plastic regime and in the elastic range. A deficiency of the model, which is however typical of classical eleastoplasticity, is that it overemphasizes the transition between the two regimes through an unrealistically abrupt change in the volumetric stiffness at yield.

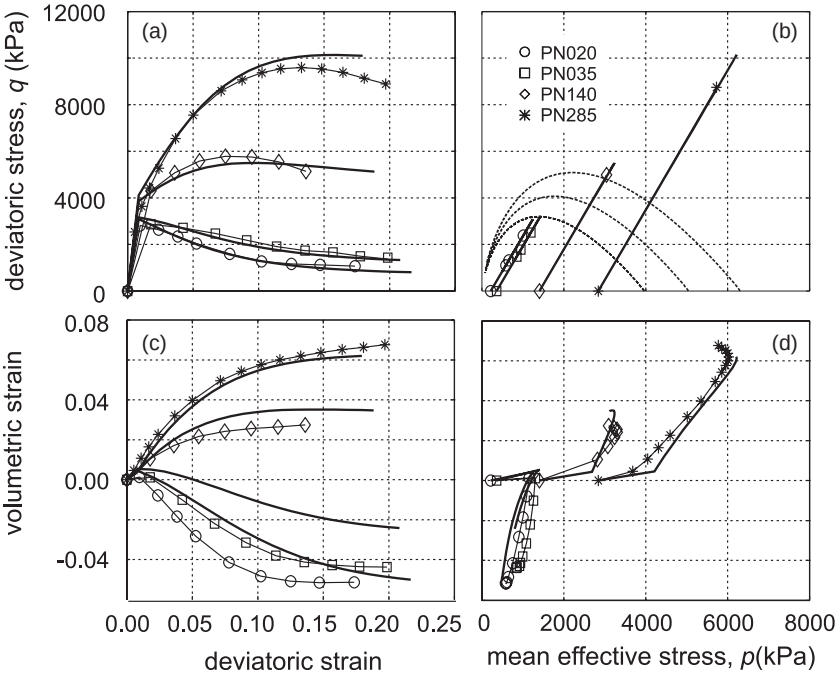

Figure 13. Drained triaxial compression; associative flow.

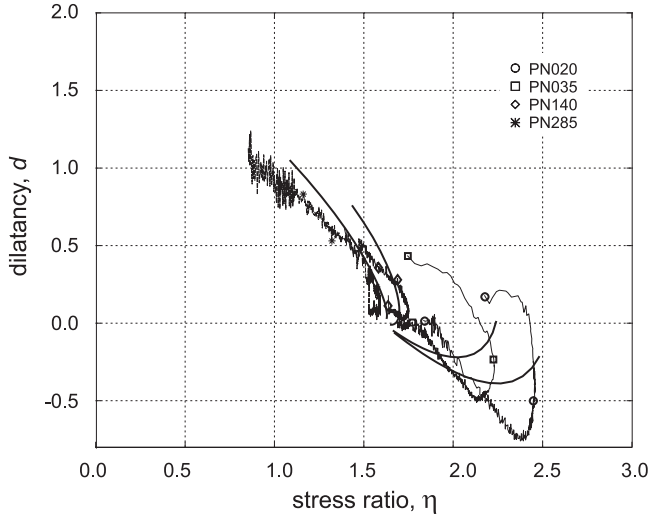

Figure 14. Stress ratio–dilatancy curves; associative flow.

The predictions for drained triaxial compression tests are given in Figures 13(a)–13(d), in the q:ε_s, q:p, ε_v:ε_s, and ε_v:p planes, respectively. In Figure 13(b), the initial positions of the yield surfaces for each specimen are also plotted.

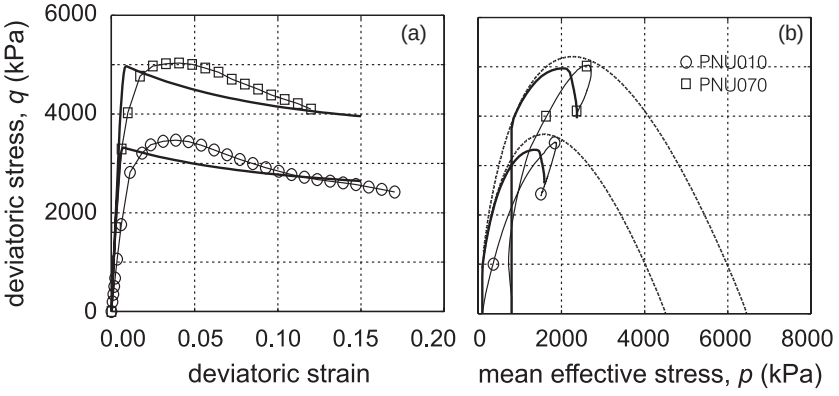

Figure 15. Undrained triaxial compression; associative flow.

Table IV. Initial state assumed in the simulations: associative case.

Test #	Test type	p_0 (kPa)	q_0 (kPa)	p_{s0} (kPa)	b_0	M_0	m_0
BPVHP	ISO	210.0	0.0	3000.0	1.8	2.3	0.9
PN020	TX–CD	214.0	0.0	2200.0	1.8	2.3	0.9
PN035	TX–CD	357.0	0.0	2200.0	1.8	2.3	0.9
PN140	TX–CD	1404.0	0.0	2800.0	1.8	2.3	0.9
PN285	TX–CD	2840.0	0.0	3500.0	1.8	2.3	0.9
PNU010	TX–CU	97.0	0.0	3000.0	1.5	2.3	0.9
PNU070	TX–CU	799.0	0.0	4300.0	1.5	2.3	0.9

In Figures 13(a) and 13(c) a good qualitative agreement between prediction and measurements can be observed. In particular, the model appears to reproduce well the transition between a fragile, dilatant behaviour at low confining stresses to a ductile, contractant behaviour at high confining stresses. At the highest confining stresses, however, the model does not capture the slight reduction in the deviatoric stress at $\varepsilon_s \simeq 0.13$, which is observed experimentally. From the quantitative point of view, the model appears to underestimate both the rate of dilation at low confining stress and the rate of contraction at the highest confining stress.

The computed stress–dilatancy curves from the drained compression tests, plotted in Figure 14, clearly show that the model succeeds in capturing, from a qualitative point of view, the characteristic shape of the experimental curves. In particular, the model correctly predicts that, at low confining stresses, the peak of the stress ratio η always precedes the point of minimum dilatancy d.

Finally, the comparison between measured and computed results for two undrained compression tests at relatively low confining stress is reported in Figure 15. Again, a good qualitative agreement with the experimental data can be noticed. The largest deviations between predictions and measurements are to be found in the shape of the stress paths in the q:p plane, see Figure 15(b). This can be due, in part to the already mentioned abrupt transition from elastic

Table V. Initial state assumed in the simulations: non-associative case

Test #	Test type	p_0 (kPa)	q_0 (kPa)	p_{s0} (kPa)	b_0 (–)	M_0 (–)	m_0 (–)
BPVHP	ISO	210.0	0.0	3000.0	1.8	2.3	1.098
PN020	TX–CD	214.0	0.0	1800.0	1.5	2.3	1.098
PN035	TX–CD	357.0	0.0	2200.0	1.5	2.3	1.098
PN140	TX–CD	1404.0	0.0	2400.0	1.5	2.3	1.098
PN285	TX–CD	2840.0	0.0	2600.0	1.55	2.3	1.098
PNU010	TX–CU	97.0	0.0	2200.0	1.5	2.3	1.098
PNU070	TX–CU	799.0	0.0	3100.0	1.5	2.3	1.098

to plastic behaviour, in part to the assumed shape of the yield locus which, in the low mean stress region, may lead to an overestimation of the deviatoric stress at yield.

4.2. Non-associative case

In the non-associative case, the main calibration problem consists in the determination of the parameters controlling the shape of the yield surface, which cannot be inferred from the stress–dilatancy data. In particular, the problem is now to determine the appropriate values for β and m_{crit} such that

$$[1 - 3\chi(\beta)]m_{\text{crit}} = \frac{d_0}{M_{\text{crit}}} \tag{48}$$

see Equations (30), (37), (45).

A qualitative indication concerning the shape of the yield function at low mean effective stress can be obtained from the shape of the measured undrained stress paths given in Figure 15(b). The rationale behind this is the following. Due to the particular geometry of the yield surface, yield loci with largely differing sizes are relatively close to each other in a neighbourhood of the origin in stress space. Therefore, even in the presence of pronounced softening, the stress path does not deviate substantially from the initial yield locus, at least as long as the changes in the value of M induced by grain crushing are not too pronounced. See, for instance, the stress–paths for the undrained tests #13–16 of Section 3.2, plotted in Figure 11.

Based on the arguments above, we have obtained the values of the material parameters listed in Table III (set #2). The initial values of the internal variables are reported in Table V. Note that the scatter in these data is now much lower than in the associative case.

The predictions for drained triaxial compression tests are given in Figures 16(a)–16(d), in the q:ε_s, q:p, ε_s:ε_v and ε_v:p planes, respectively. The corresponding stress–dilatancy curves are shown in Figure 17. As in the associative case, a good qualitative agreement with measurements is observed. In addition, the model is now able to capture the experimentally observed peak in the q:ε_s curves for the tests at higher confining stresses.

The main observed effect of non-associativity is in the predicted dilatancy, see Figure 16(c) and 17. As compared to the associative case, the predicted behaviour at high stress levels is now characterized by a higher contractancy, as indicated by the stress–dilatancy curves of Figure 17. This effect is due to the much larger value of a which has been adopted in the non-associative

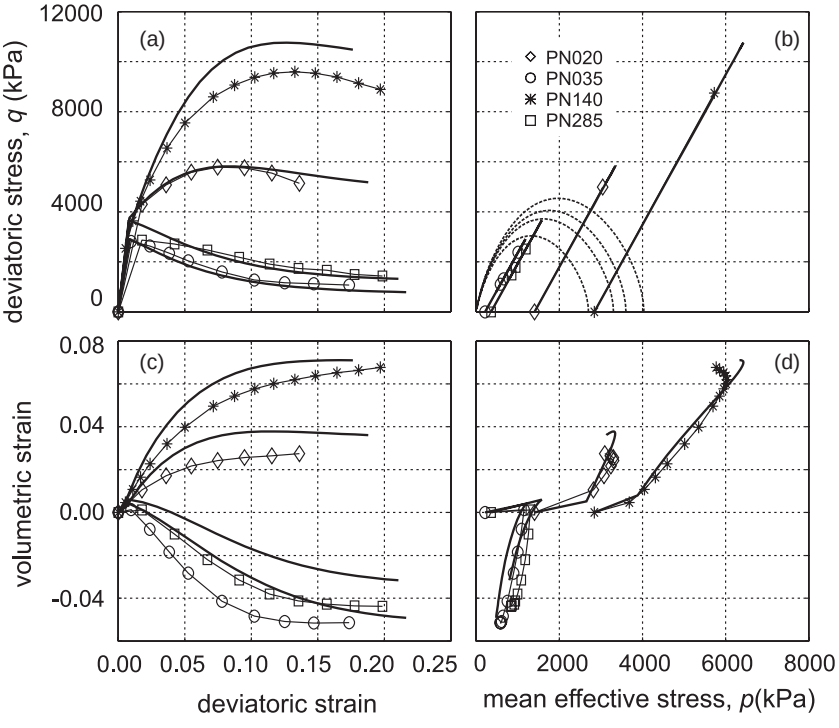

Figure 16. Drained triaxial compression; non-associative flow.

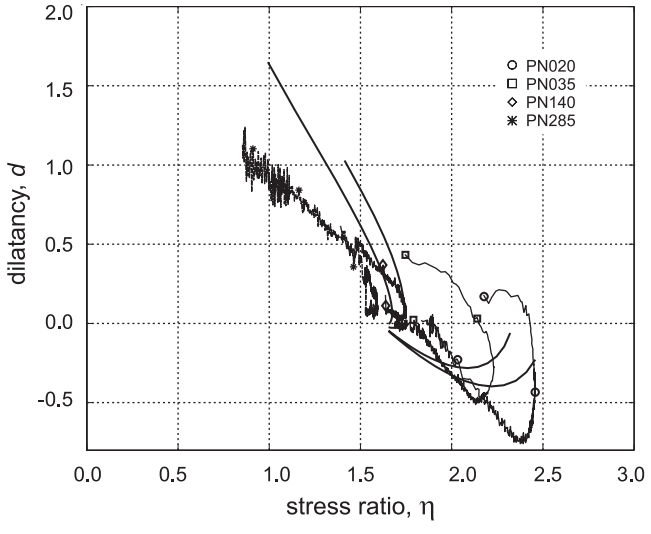

Figure 17. Stress ratio–dilatancy curves; non-associative flow.

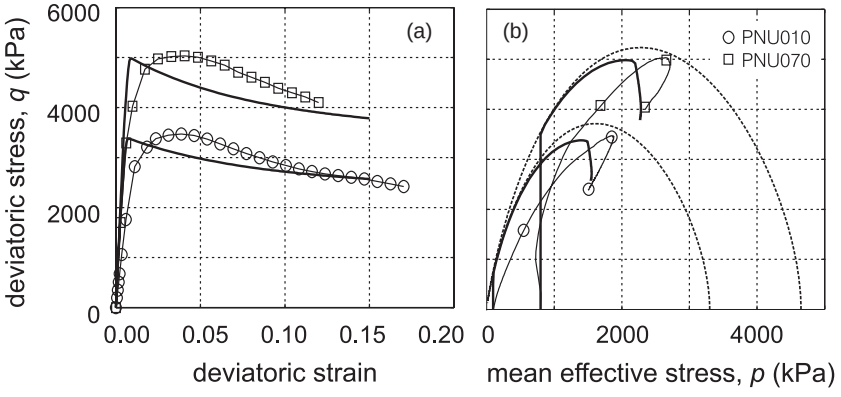

Figure 18. Undrained triaxial compression; non-associative flow.

case (see Table III), in order to improve the predictions for TX–CU tests PNU010 and PNU070 discussed below.

As for the undrained tests, reported in Figure 18, non-associativity has some impact on the shape of predicted stress–paths, which is a consequence of the different shape of the yield loci—compare Figures 13(b) and 16(b). The corresponding stress–strain curves, however, show no substantial differences.

5. CONCLUDING REMARKS

In this paper, a constitutive model for granular soils undergoing grain crushing has been developed in the framework of classical isotropic hardening plasticity, based on the following fundamental assumptions:

(i) grain crushing induces a reduction in the frictional properties of the material which is accounted for by considering the stress ratio at zero dilatancy, M, as an internal variable which degrades with accumulated plastic strain;
(ii) grain crushing has also an effect on the shape of the yield locus, which is indirectly described through the observed changes of the stress–dilatancy curves. This effect is introduced in the formulation by treating parameter m of the yield function as an additional internal variable, the evolution of which is a function of the plastic strain rate invariants;
(iii) finally, a third effect of grain crushing is the progressive downward shift of the virgin compression line in the ε_v: $\ln p$ plane, which is modelled by introducing a further internal variable b representing the ratio between the current size of the yield locus in isotropic compression and the size p_s corresponding to the stable, fully degraded material.

One of the salient features of the proposed model is its capability of describing a stress–dilatancy relationship in which the minimum value of dilatancy does not correspond to the maximum stress ratio experienced by the material.

Although in its present formulation the model does not account for the mechanical effects of intergranular bonding (e.g. cementation), the inclusion of this feature is straightforward by following the approach outlined, e.g. in Reference [5].

The applicability of the proposed model to natural soils has been demonstrated by comparing its predictions to the observed behaviour of a pyroclastic weak rock (Pozzolana Nera). Taking into account the intrinsic small-scale heterogeneity of the natural material, the agreement between predictions and measurements appears satisfactory even in the case of associative flow rule. Although Pozzolana Nera does exhibit some true cohesion originating from weak interparticle bonds, the model is still capable of providing a good match with experimental observation. This is possibly due to the comparatively high stress levels at which tests were performed. There are, however, important engineering applications, such as stability analysis of open cuts, in which the stress levels of practical interest are much lower. In these cases, interparticle bonding may play a major role [46].

ACKNOWLEDGEMENT

Part of this work was carried out during visits by MC, CT and GMBV to the Max Planck Institute for Mathematics in the Sciences in Leipzig. The hospitality and support from this Institution is gratefully acknowledged.

APPENDIX A

To integrate numerically the differential-algebraic system given by Equations (4)–(7) along the different loading paths considered in Sections 3 and 4, an adaptive, embedded Runge–Kutta–Fehlberg method of order 2 and 3 [47] has been employed in connection with an algorithm to simulate generalized loading paths first proposed by Bardet and Choucair [42].

In their method, Bardet and Choucair consider a generalized loading condition in which the imposed constraints on arbitrary components of both stress and strain tensors and the prescribed time history on one of such components chosen as a control variable can be cast in linearized form as follows:

$$\mathbf{S}\dot{\boldsymbol{\sigma}} + \mathbf{E}\dot{\boldsymbol{\varepsilon}} = \mathbf{V} \tag{A1}$$

where $\mathbf{E}$ and $\mathbf{S}$ are suitable 6×6 *constraint matrices*, depending on the imposed loading path, $\mathbf{V}$ is a *loading rate vector*, defined as

$$\mathbf{V} := \{0 \;\; 0 \;\; 0 \;\; 0 \;\; 0 \;\; V\} \tag{A2}$$

and V is the (prescribed) loading rate imposed to the control variable. In Equation (50), $\dot{\boldsymbol{\varepsilon}}$ and $\dot{\boldsymbol{\sigma}}$ denote the stress and strain rates now represented as six-dimensional vectors. By an appropriate choice of the coefficients of matrices $\mathbf{E}$ and $\mathbf{S}$, Equation (A1) can describe the loading conditions imposed in practically all currently available testing equipments, from stress–path controlled triaxial cells to true triaxial apparati or hollow cylinders (see Reference [42] for details).

From Equations (4), (5) and $(15)_2$, the stress rate can be expressed as a function of the strain rate as

$$\dot{\boldsymbol{\sigma}} = \mathbf{D}(\boldsymbol{\sigma}, \mathbf{q}, \boldsymbol{\eta}_\varepsilon)\dot{\boldsymbol{\varepsilon}} \;\; \mathbf{D} := \mathbf{D}^{\mathrm{e}} - \frac{\bar{h}(\dot{\gamma})}{K_p}(\mathbf{D}^{\mathrm{e}}\mathbf{Q}) \otimes (\mathbf{P}^{\mathrm{T}}\mathbf{D}^{\mathrm{e}}) \tag{A3}$$

in which K_p and $\mathbf{Q}$ are given by Equations (14) and (29), respectively, $\mathbf{P} \coloneqq \partial f/\partial \boldsymbol{\sigma}$ is the gradient of the yield function, $\dot{\gamma}$ is the plastic multiplier given by Equation (15), and $\hbar(x)$ is the Heaviside step function, equal to 1 when $x > 0$ and equal to 0 otherwise.

Taking into account the constitutive equation $(51)_1$, Equation (49) transforms in

$$\mathbf{A}\dot{\boldsymbol{\varepsilon}} = \mathbf{V}, \ \mathbf{A} \coloneqq \mathbf{SD} + \mathbf{E} \tag{A4}$$

If the loading conditions are properly set in order to guarantee controllability (see Reference [48]), matrix $\mathbf{A}$ is non-singular, and the strain rate can be obtained as

$$\dot{\boldsymbol{\varepsilon}} = \mathbf{A}^{-1}\mathbf{V} \tag{A5}$$

The original problem of evolution given by Equations (4)–(6) can thus be reformulated, to take into account the imposed loading condition, in the following compact form:

$$\dot{\mathbf{y}} = \mathbf{f}(\mathbf{y}) \tag{A6}$$

in which

$$\mathbf{y} \coloneqq \begin{Bmatrix} \boldsymbol{\varepsilon} \\ \boldsymbol{\sigma} \\ \mathbf{q} \\ \boldsymbol{\varepsilon}^{\mathrm{p}} \end{Bmatrix} \quad \mathbf{f}(\mathbf{y}) \coloneqq \begin{Bmatrix} \mathbf{A}^{-1}\mathbf{V} \\ \mathbf{D}\mathbf{A}^{-1}\mathbf{V} \\ (1/K_p)\langle \mathbf{P}^{\mathrm{T}}\mathbf{D}^{\mathrm{e}}\mathbf{A}^{-1}\mathbf{V}\rangle \mathbf{h} \\ (1/K_p)\langle \mathbf{P}^{\mathrm{T}}\mathbf{D}^{\mathrm{e}}\mathbf{A}^{-1}\mathbf{V}\rangle \mathbf{Q} \end{Bmatrix} \tag{A7}$$

Equation (A6) is a canonical system of ODEs. An accurate and efficient way to solve it is to adopt an embedded Runge–Kutta–Fehlberg method of order 2 and 3 (RKF–23, see, e.g. Reference [47]).

Let $\mathbb{I} = \bigcup_{n=0}^{N} [t_n, t_{n+1}]$ be a partition of the time interval of interest $[t_0, t_{\mathrm{fin}}]$ into time steps. It is assumed that, at time $t_n \in \mathbb{I}$, the vector $\mathbf{y}_n$ is known and the loading rate $\mathbf{V}$ is given. The computational problem to be addressed is to find the update $\mathbf{y}_{n+1}$ of $\mathbf{y}$ at $t = t_{n+1}$. To this end, define a non-dimensional time scale $T = (t - t_0)/(t_{\mathrm{fin}} - t_0)$, so that $\Delta T_n \coloneqq T_{n+1} - T_n = (t_{n+1} - t_n)/(t_{\mathrm{fin}} - t_0)$ and $\sum_{n=0}^{N} \Delta T_n = 1$, and let

$$\tilde{\mathbf{y}}_{n+1} = \mathbf{y}_n + \Delta T_n \sum_{j=1}^{\tilde{N}} \tilde{C}_j \mathbf{k}_j(\mathbf{y}_n, \Delta T_n) \tag{A8}$$

$$\hat{\mathbf{y}}_{n+1} = \mathbf{y}_n + \Delta T_n \sum_{j=1}^{\hat{N}} \hat{C}_j \mathbf{k}_j(\mathbf{y}_n, \Delta T_n) \tag{A9}$$

be the recurrence formulas provided by explicit Runge–Kutta methods of order $\tilde{N} = 2$ and $\hat{N} = \tilde{N} + 1 = 3$, respectively, where $\tilde{C}_1 = 0$, $\tilde{C}_2 = 1$, $\hat{C}_1 = \hat{C}_3 = 1/6$, and:

$$\mathbf{k}_1 \coloneqq \mathbf{f}(\mathbf{y}_n) \tag{A10}$$

$$\mathbf{k}_2 \coloneqq \mathbf{f}\left(\mathbf{y}_n + \frac{1}{2}\Delta T_n \mathbf{k}_1\right) \tag{A11}$$

$$\mathbf{k}_3 \coloneqq \mathbf{f}(\mathbf{y}_n - \Delta T_n \mathbf{k}_1 + 2\Delta T_n \mathbf{k}_2) \tag{A12}$$

see Reference [47]. Since the two approximations to the unknown value of $\mathbf{y}(t_{n+1})$ have different global convergence order, an adaptive step size control strategy which allows to keep the integration error below a prescribed tolerance can be defined as follows. Consider the following *relative error* vector:

$$\mathbf{R}_{n+1} := \left\{ \begin{array}{c} (\hat{\boldsymbol{\varepsilon}}_{n+1} - \tilde{\boldsymbol{\varepsilon}}_{n+1})/\|\hat{\boldsymbol{\varepsilon}}_{n+1}\| \\ (\hat{\boldsymbol{\sigma}}_{n+1} - \tilde{\boldsymbol{\sigma}}_{n+1})/\|\hat{\boldsymbol{\sigma}}_{n+1}\| \\ (\hat{\mathbf{q}}_{n+1} - \tilde{\mathbf{q}}_{n+1})/\|\hat{\mathbf{q}}_{n+1}\| \\ (\hat{\boldsymbol{\varepsilon}}^{\mathrm{p}}_{n+1} - \tilde{\boldsymbol{\varepsilon}}^{\mathrm{p}}_{n+1})/\|\hat{\boldsymbol{\varepsilon}}^{\mathrm{p}}_{n+1}\| \end{array} \right\} \tag{A13}$$

If $\|\mathbf{R}_{n+1}\| < \mathrm{TOL}$, where TOL is a prescribed relative error tolerance, then the solution given by the third order method, Equation (A9), is accepted, and a (larger) time step size for the next step is computed according to the following extrapolation formula:

$$\Delta T_{n+1} = \min\left\{ 0.9\Delta T_n \left[\frac{\mathrm{TOL}}{\|\mathbf{R}_{n+1}\|} \right]^{1/3} ; 4\Delta T_n \right\} \tag{A14}$$

If, on the contrary, $\|\mathbf{R}_{n+1}\| \geqslant \mathrm{TOL}$, then the time step is rejected, and a new, smaller time step size is evaluated as:

$$\Delta T_n \leftarrow \max\left\{ 0.9\Delta T_n \left[\frac{\mathrm{TOL}}{\|\mathbf{R}_{n+1}\|} \right]^{1/3} ; \frac{1}{4}\Delta T_n \right\} \tag{A15}$$

and the integration is repeated until the prescribed accuracy is met. In all the numerical simulations presented in Sections 3 and 4, a value of $\mathrm{TOL} = 1.0 \times 10^{-2}$ has been employed.

REFERENCES

1. Aversa S. Mechanical behaviour of soft rock: some remarks. In: *Experimental Characterisation and Modelling of Soils and Soft Rocks*. CUEN: Napoli, Italy, 1991; 191–223.
2. Cecconi M, Viggiani GMB. Structural features and mechanical behaviour of a pyroclastic weak rock. *International Journal for Numerical and Analytical Methods in Geomechanics* 2001; **25**(15):1525–1557.
3. Coop MR. The influence of particle breakage and state on the behaviour of sands. In: *International Workshop on Soil Crushability*, *IWSC'99*, Yamaguchi, Japan, 2000. Japan Geotechnical Society.
4. Cuccovillo T. Shear behaviour and stiffness of naturally cemented sands. *PhD Thesis*, City University of London, 1995.
5. Lagioia R, Nova R. An experimental and theoretical study of the behaviour of a calcarenite in triaxial compression. *Géotechnique* 1995; **45**(4):633–648.
6. Fukumoto T. A grading equation for decomposed granite soil. *Soils and Foundations* 1990; **30**(1):27–34.
7. Lee IK. The mechanical behaviour of compacted decomposed granite. *PhD Thesis*, City University of London, 1991.
8. Nova R. Mathematical modelling of natural and engineered geomaterials. *European Journal of Mechanics A/Solids* (special issue) 1992; **11**:135–154.
9. Gens A, Nova R. Conceptual bases for a constitutive model for bonded soils and weak rocks. In: *Hard Soils–Soft Rocks*, Anagnostopoulos *et al.* (eds.) Balkema: Rotterdam, Athens, Greece, 1993.
10. Kavvadas M. On the mechanical behaviour of bonded soils. In *COMETT Seminar on Large Excavations*, 1994.
11. Wood DM. Kinematic hardening model for structured soil. In: *NUMOG V*, Pande GN, Pietrusczczak S (eds.) Balkema: Rotterdam, 1995; p. 83–88.
12. Rouainia M, Muir Wood D. A kinematic hardening constitutive model for natural clays with loss of structure. *Géotechnique* 2000; **50**(2):153–164.
13. Gajo A, Muir Wood D. A new approach to anisotropic bounding surface plasticity: general formulation and simulations of natural and reconstituted clay behaviour. *International Journal for Numerical and Analytical Methods in Geomechanics* 2001; **25**:207–241.
14. Elliott GM, Brown ET. Yield of a soft, high porosity rock. *Géotechnique* 1985; **35**(4):413–423.
15. Airey DW. Triaxial testing on naturally cemented carbonate soil. *Journal of Geotechnical Engineering*, *ASCE* 1993; **119**(9):1379–1398.

16. Aversa S, Evangelista A. The mechanical behaviour of a pyroclastic rock: yield strength and destructuration effects. *Rock Mechanics and Rock Engineering* 1998; **31**(1):25–42.
17. Maccarini M. Laboratory studies of a weakly bonded artificial soil. *PhD Thesis*. Imperial College of Science Technology and Medicine, University of London, 1987.
18. Leroueil S, Vaughan PR. The general and congruent effects of structure in natural soils and weak rocks. *Géotechnique* 1990; **40**(3):467–488.
19. Cotecchia F, Chandler RJ. The influence of structure on the pre-failure behaviour of a natural clay. *Géotechnique*, 1990; **47**(3):523–544.
20. Herle I, Gudehus G. Determination of parameters of a hypoplastic constitutive model from properties of grain assemblies. *Mechanics of Cohesive–Frictional Materials* 1999; **4**:461–486.
21. Miura K, Maeda K, Toki S. Method of measurement for the angle of repose of sands. *Soils and Foundations* 1997; **37**(2):89–96.
22. Li XS, Dafalias YF. Dilatancy for cohesionless soils. *Géotechnique* 2000; **50**(4):449–460.
23. Miura N, O-Hara S. Particle-crushing of a decomposed granite soil under shear stresses. *Soils and Foundations* 1979; **19**(3):1–13.
24. Hardin BO. Crushing of soil particles. *Journal of Geotechnical Engineering*, *ASCE* 1985; **111**(10):1177–1192.
25. Hagerty MM, Hide DR, Ullrich CR, Hagerty DJ. One-dimensional high-pressure compression of granular media. *Journal of Geotechnical Engineering*, *ASCE*, 1993; **119**(1):1–18.
26. Lade PV, Yamamuro JA, Bopp PA. Significance of particle crushing in granular materials. *Journal of Geotechnical Engineering*, *ASCE* 1996; **122**(4):309–316.
27. Nakata Y, Hyodo M, Hyde AFL, Kato Y, Murata H. Microscopic particle crushing of sand subjected to high pressure one dimensional compression. *Soils and Foundations* 2001; **41**(1):69–82.
28. Nakata Y, Kato Y, Hyodo M, Hyde AFL, Murata H. One dimensional compression behaviour of uniform sand related to single particle crushing strength. *Soils and Foundations* 2001; **41**(2):39–51.
29. McDowell GR, Bolton M. On the micromechanics of crushable aggregates. *Géotechnique* 1998; **48**(5):667–679.
30. McDowell GR. A family of yield loci based on micromechanics. *Soils and Foundations* 2000; **40**(6):133–137.
31. Simo JC, Hughes TJR. *Computational Inelasticity*. Springer Verlag: New York, 1997.
32. Houlsby GT. The use of a variable shear modulus in elastic–plastic models for clays. *Computers and Geotechnics* 1985; **1**:3–13.
33. Lagioia R, Puzrin AM, Potts DM. A new versatile expression for yield and plastic potential surfaces. *Computers and Geotechnics* 1996; **19**:171–191.
34. van Eekelen HAM. Isotropic yield surfaces in three dimensions for use in soil mechanics. *International Journal for Numerical and Analytical Methods in Geomechanics* 1980; **4**:89–101.
35. Nova R. Sinfonietta classica: an exercise on classical soil modelling. In: *Constitutive Equations for Granular Non-Cohesive Soils*, Saada AS, Bianchini GF (eds.), Balkema: Rotterdam, Cleveland, 1988.
36. Sture S, Runesson K, Macari-Pasqualino EJ. Analysis and calibration of a three-invariant plasticity model for granular materials. *Ingenieur–Archiv* 1989; **59**:253–266.
37. Runesson K. Implicit integration of elastoplastic relations with reference to soils. *International Journal for Numerical and Analytical Methods in Geomechanics* 1987; **11**:315–321.
38. Alawaji H, Runesson K, Sture S. Implicit integration in soil plasticity under mixed control for drained and undrained response. *International Journal for Numerical and Analytical Methods in Geomechanics* 1992; **16**: 737–756.
39. Nova R, Wood DM. A constitutive model for sand in triaxial compression. *International Journal for Numerical and Analytical Methods in Geomechanics* 1979; **3**:255–278.
40. Nova R. On the hardening of soils. *Archiwum Mechaniki Stosowanej* 1977; **29**:445–458.
41. Fuller WB, Thompson SE. The laws of proportioning concrete. *Transactions on ASCE* 1907; **59**:67–172.
42. Bardet JP, Choucair W. A linearized integration technique for incremental constitutive equations. *International Journal for Numerical and Analytical Methods in Geomechanics* 1991; **15**:1–19.
43. Taylor DW. *Fundamentals of Soil Mechanics*. Wiley: New York, 1948.
44. Rowe PW. The stress–dilatancy relation for static equilibrium of an assembly of particles in contact. *Proceedings of the Royal Society of London* 1962; **A269**:500–527.
45. Cecconi M. Caratteristiche strutturali e proprietà meccaniche di una piroclastite: la Pozzolana Nera dell'area romana. *PhD Thesis*, Università di Roma "Tor Vergata", 1999 (in Italian).
46. Cecconi M, Viggiani GMB. Stability of subvertical cuts in pyroclastic deposits. In *Proceedings Geoeng 2000*, Melbourne, Australia, 2000.
47. Stoer J, Bulirsch R. *Introduction to Numerical Analysis* (2nd edn). Springer Verlag: New York, 1992.
48. Nova R. Controllability of the incremental response of soil specimens subjected to arbitrary loading programmes. *Journal of Mechanical Behaviour of Materials* 1994; **5**(2):193–201.

